Hindawi
Applied and Environmental Soil Science
Volume 2023, Article ID 6856144, 18 pages
https://doi.org/10.1155/2023/6856144

*Research Article*

# The Response of Sensitive LULC Changes to Runoff and Sediment Yield in a Semihumid Urban Watershed of the Upper Awash Subbasin Using the SWAT+ Model, Oromia, Ethiopia

**Bekan Chelkeba Tumsa**

*Faculty of Civil and Environmental Engineering, Jimma Institute of Technology, Oromia, Ethiopia*

Correspondence should be addressed to Bekan Chelkeba Tumsa; bekanchelkeba@gmail.com

Received 28 October 2022; Revised 30 December 2022; Accepted 12 January 2023; Published 31 January 2023

Academic Editor: Oliver Dilly



Land use and land cover (LULC) changes in many parts of river basins have caused water shortages, flood risks, land degradation, soil loss, biodiversity loss, and ecosystem deterioration. LULC change and topography are the main factors that cause land degradation and soil erosion in the Ethiopian highlands. The aim was to evaluate the rate of the LULC change and its effects on runoff and sediment yield in the semihumid subtropical Awash watershed using the SWAT + model. The land use maps of 2000, 2010, and 2020, along with constant climate data from 1992 to 2020, were used to investigate the effects of LULC dynamics on runoff and sediment yields. Agriculture and urbanization both increased at 7.1% and 7.95%, respectively. In contrast, the forest area decreased by 8.8% and shrubland by 3.25% from 2000 to 2020. Bare soil and urban areas covered the majority of the landscape units that were labeled as potential runoff generators. The majority of the soil erosion-prone areas that were classified as severe in the second and third scenarios covered a sizable area of urban, agricultural, and shrubland. These soil erosion hotspots covered an area of 3,777.3 ha (3.18%) and 13,413.1 ha (11.3%), with a total annual sediment yield of 361.93 m/ton and 1239.24 m/ton, respectively. In general, the change in LULC results in the annual sediment yield, with mean annual amounts of 241.8 tons/ha, 408.7 tons/ha, and 732.4 tons/ha for each scenario in the sequence. The model performance was tested using $R^2 = 0.88$, NSE = 0.9, and PBIAS = −2.36, which indicate good agreement between simulated and observed flow, and $R^2 = 0.82$, NSE = 0.86, and PBIAS = 4.38 for the simulated against recorded sediment yield. The increases in sediment yields have serious implications for reservoir siltation downstream of the watershed and warn land use managers to take action.

## 1. Introduction

On a local and global scale, the interaction of demographic settings and socioeconomic variables is the primary driver of environmental changes and ecosystem depletion [1]. Land use and cover dynamics have been major sources of soil erosion, surface runoff, and sediment yields in recent times [2]. The changes in land use and land cover have played a significant role in varying runoff, water yields, soil erosion, and sediment yields in many river basins [3]. Because of the conversion of forest to agricultural and other land uses, the watershed has become prone to soil erosion [1]. The shift in land use begins in regions with high socioeconomic activity and population income based on agriculture, particularly in Africa [4]. Land users are engaged in destructive anthropogenic processes such as deforestation during the land expansion for agricultural activities [5]. As a result of land degradation and soil erosion, approximately 75 billion metric tons of soil have been removed worldwide each year [6].

Land degradation in Ethiopia has resulted from intentional soil erosion caused by land use and cover change due to overgrazing, urban expansion, deforestation, and growing agricultural business [7]. This soil erosion, in turn, exposed downstream watershed regions to high sediment yields and gradually raised the bed level of hydraulic schemes [8]. Furthermore, the sediment yield is the most serious issue in Ethiopia's subwatershed regions and

ecosystems [9]. Most infrastructures, like irrigation canals, reservoirs, and water intake structures, have been damaged by annual sediment deposition [10]. For these reasons, a comprehensive understanding of the consequences of urban expansion and changes in land use and land cover is required to identify an optional mitigation measure for the protection of floods and sediment accumulation to enhance sustainable water resource management [11].

According to a few studies, agricultural land expansion due to deforestation has resulted in soil erosion, runoff, and sediment yields and is considered a major cause of land degradation and environmental changes [12]. Population density causes high pressure on land resources which drive to land use and land cover change, according to research conducted on the upper Awash River basin [13]. Other research evidence indicates that approximately 27 million hectares of Ethiopian lands have been eroded, and many catchments are vulnerable to soil erosion and sediment yields beyond reclamation [14]. The highlands of Ethiopia, in particular, the upper Blue Nile and Awash River basins, have been severely degraded and are regarded as the region subjected to the highest rate of soil erosion, runoff, and sedimentation downstream of river basins [15, 16].

The purpose of this study was to identify the runoff and sediment yield with erosion-prone areas that contribute sediment yields to the downstream using the SWAT + model. This model is a restructured version that can analyze catchment hydrology at the landscape units (LSUs) and HRU levels by integrating into the subwatershed level through a modified routing system that uses QSWAT+ [17].

## 2. Materials and Methods

*2.1. Description of the Study Area.* The Big Akaki catchment is located in the west of Addis Ababa, while the Little Akaki catchment is located in the east. Both rivers flow into the Abba Samuel reservoir, which generates 6.6 MW of hydropower and serves local agricultural communities. This watershed is distinguished by a variety of topographic conditions ranging from flat plains to steep areas. The catchment is in the upper Awash subbasin, which is geographically located at latitudes of 8° 46′ to 9° 14′ north latitude and longitudes of 38° 34′ to 39° 04′ east, and covers a total area of 1187 $km^2$, as shown in Figure 1.

*2.2. Topography of the Area.* According to DEM data analysis, both catchments in the watershed have a simple landscape with a various topographical features, including medium mountainous to flat plains, hills, and plateaus. The upper reaches are plateaus with mountains, while the middle region has steep and moderate gorges and the lower basin is flat. The western parts of the watershed have basalt with shallow aquifers and are extremely vulnerable to the erosive activities of the surrounding rivers [18]. In general, the slope of each catchment varies from gentle to steeper at the outlet and in the middle of the watershed respectively. This varying slope from steeper to midlist allows for high sediment accumulation in the middle and lower portions of the Awash sub-basins [19].

*2.3. Climate.* The upper Awash subwatershed is situated in a semihumid climate, and the average minimum and maximum temperatures are in the range of 7°C to 11°C and 21°C to 28°C, respectively [20]. The lowest temperature recorded in the area was 7°C in November and December, and the highest was 28°C in March and May. The main rainy season was from late June to early September, with the dry season occurring in December, January, February, and mid-March. The average annual rainfall in this area is 1965 mm, and the plotted rainfall intensity recorded at all stations in the study area is shown in Figure 2.

*2.4. Meteorological and Hydrological Data.* This research made use of both spatial and time-series data. DEM, soil, and Landsat images from three periods were acquired and used for spatial analysis with ArcGIS. Climate data from six synoptic stations were used for the SWAT + model input. For model calibration and validation, streamflow and sediment data were collected from the Ministry of Water, Irrigation, and Electricity (MoWIE), as shown in Table 1. DEM with a resolution of (12.5 m × 12.5 m) was used to analyze the drainage patterns of the watershed terrains. River discharge is affected by seasonal rainfall variability, and the mean monthly flow at the confluence points of both catchments ranges from 42.7 $m^3/s$ to 80.5 $m^3/s$.

*2.5. Classification of Soil.* The study area's soil classification has been divided into six soil groups. Soil characteristics determine how rainfall, runoff, and river flow react to them, causing soil erosion and sedimentation. SWAT+ and other hydrological models require soils of various types, textures, colours, moisture contents, hydraulic conductivity, and organic content [21]. The Akaki watershed is dominated by six soil types, which are expected to cause soil erosion and runoff. As shown in Table 2, Pellic vertisols dominate this watershed, covering 55% of the area [22].

*2.6. LULC Classifications.* Akaki catchments' land use and land cover patterns are changing over time, from agricultural land to built-up areas and sparse forest to shrubland, affecting hydrological processes and ecosystem functions. The catchment is dominated by urban and agricultural lands for the most part. Furthermore, the dynamic of this land cover is causing soil erosion and sediment loading in the rivers' downstream sections. Water bodies, sparse forests, bare soils, agriculture, wetland, and shrubland cover much of the catchment. Since 2000, the rate of land use change in this area has shown progressive variability [23]. This study uses ERDAS-2015 software to classify images from three years of multispectral satellite imagery composed of different bands from three Landsat images, as shown in Table 3. The annual rate of change in land use and land cover from 2000 to 2010 and 2010 to 2020 has been calculated using Equation (2).

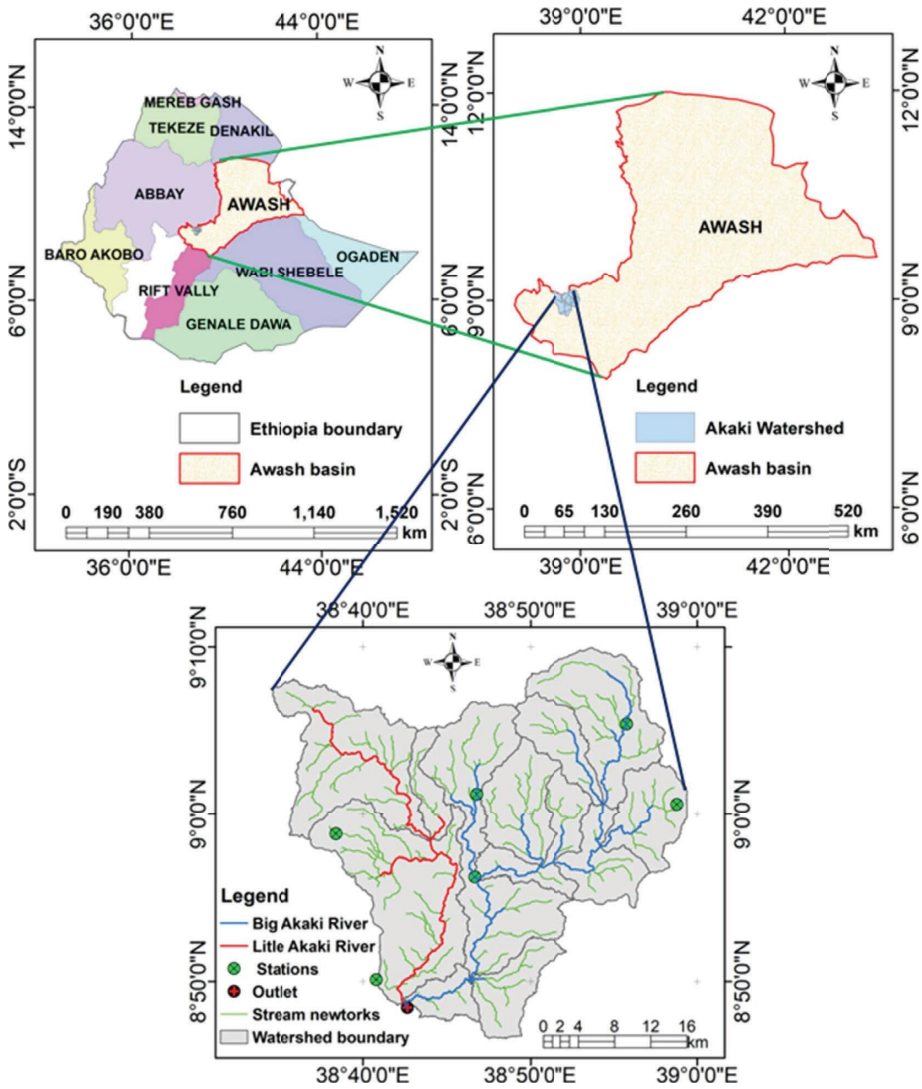


Figure 1: Map of the study area.

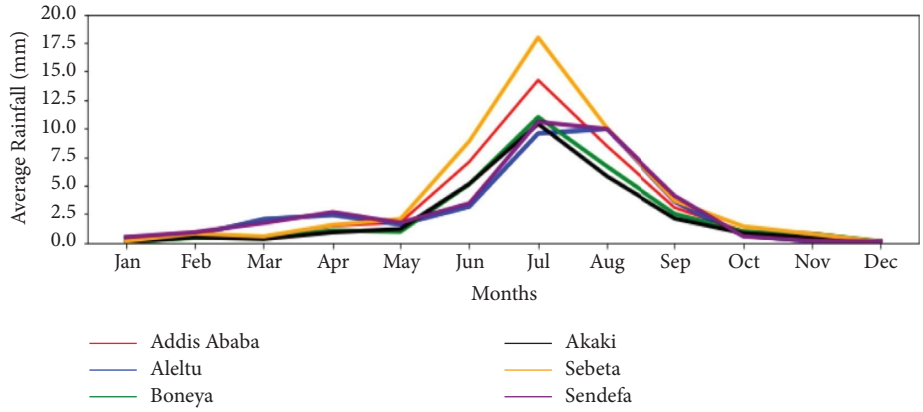


Figure 2: Monthly average rainfall intensity at each station.

*2.7. Image Classification and Accuracy Assessment.* Supervised classification is the most important and widely used technique in multispectral satellite image classification [24]. All pixel cell images are automatically classified and compared to multispectral values for land use and land cover classes to use them as an input to the SWAT + model [25]. In this study, 203 ground points were taken to increase the accuracy of image classification to its ground truth of land

Table 1: Data sources and types.

| Data types | Stations | Length of records | Source of data |
|---|---|---|---|
| Meteorological data | Addis Ababa<br>Boneya<br>Akaki<br>Sabata<br>Aleltu<br>Sendefa | 1992–2020 | Ethiopia NMA |
| Streamflow data | At outlets | 1992–2020 | Ethiopia MoWIE |
| Sediment data | At outlets | 1997–2020 | |
| Soil data | | 2013 | |

Table 2: The dominant soil classes in the study area and their SWAT + codes.

| No. | Soil types | SWAT + code | Area ($km^2$) | Percentage (%) |
|---|---|---|---|---|
| 1 | Vertic Cambisols | Bv | 51 | 4.30 |
| 2 | Eutric Nitisols | Ne | 151 | 12.72 |
| 3 | Orthic Solonchaks | Zo | 91 | 7.67 |
| 4 | Calcic Xerosols | Xk | 53 | 4.47 |
| 5 | Pellic Vertisols | Vp | 655 | 55.18 |
| 6 | Chromic Vertisols | Vc | 185 | 15.59 |

Table 3: Data from satellite imaging.

| Years | Spacecraft | Sensor ID | Path/row | Acquisition date (dd/mm/yy) | Resolution |
|---|---|---|---|---|---|
| 2000 | Landsat 7 | ETM+ | 169/055 | 15/12/2001 | 30 m ∗ 30 m |
| 2010 | Landsat 8 | OLI-TIRS | 170/054 | 15/04/2012 | 15 m ∗ 15 m |
| 2020 | Landsat 8 | OCR | 169/055 | 31/01/2020 | 15 m ∗ 15 m |

cover classes. The more the ground points are, the more the image is accurate to be classified, as the image processing procedure diagram shown in Figure 3 and Table 4. The user's accuracy, the producer's accuracy, and the kappa coefficient statistics ($K$) were used to assess the accuracy of the final image classification for the SWAT + input, as shown in Table 5.

$$k = \frac{N\sum_{i=1}^{r} X_{ii} - \sum_{i=1}^{r}\left(X_{i+} * X_{1+}\right)}{N^2 - \sum_{i=1}^{r}\left(X_{i+} * X_{i+}\right)}$$

$$\text{Overall accuracy} = \frac{\text{number of points correctly classified}}{\text{total number of points classified}}, \quad (1)$$

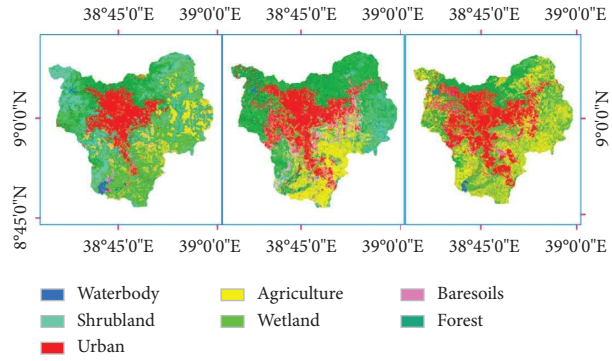


Figure 3: Land use and cover maps for 2000, 2010, and 2020.

where $N$ is the total number of sites in the matrix, $r$ is the number of rows in the matrix, $X_{ii}$ is the number in rows $i$ and columns $i$, $X_{i+1}$ is the total for rows $i$, and $X_{i+}$ is the total for the columns.

$$r = \left(\frac{1}{t_2 - t_1}\right)x \quad \ln\left(\frac{A_2}{A_1}\right), \quad (2)$$

where $r$ is the change for each class per year, $A_2$ and $A_1$ are the class areas at the end and the beginnings of years, respectively, for the period being evaluated, and $t$ is the number of years spanning that period.

## 3. Methodology

*3.1. Relationship between Streamflow and Sediment Yields.* The SWAT model divides the hydrology of a watershed into the routing phases of the hydrologic cycle [26]. The land phase of the hydrologic cycle regulates the amount of water, sediment, nutrients, and pesticides that enter the main channel. SWAT+ calculates water, sediment, and nutrient transformations and losses at each HRU level. These are then aggregated at the subbasin level and routed to the catchment outlet through the channel network [27]. The water balance equation shown in Equation (3) serves as the foundation for this model [11]. The overall methodological flow is shown in Figure 4.

$$SW_t = SW_0 + \sum_{i=1}^{t}\left(R_{\text{day}} - Q_{\text{sur}} - E_a - W_{\text{seep}} - Q_{gw}\right), \quad (3)$$

where $S_{Wt}$ is the soil water content (mm), $S_{Wo}$ is the soil water content on a day $i$ (mm), $t$ is the time (days), $R_{\text{day}}$ is the precipitation on the day $i$ (mm), $Q_{\text{Surf}}$ is the surface runoff on the day $i$ (mm), $E_a$ is the evapotranspiration on the day $i$ (mm), $W_{\text{Seep}}$ is the water entering the vadose zone from the soil profile on the day $i$ (mm), and $Q_{gw}$ is the return flow on the day $i$ (mm).

SWAT+ can also estimate sediment loads using the Modified Universal Soil Loss Equation (MUSLE), which is generated from a watershed and is based on the soil loss equation developed by [28], as shown in Equation (4). Nevertheless, surface runoff is calculated using the SCS curve number method as given in Equation (5).

Table 4: Land use and land cover map confusion matrix.

| Name | WATL | RNGB | URBN | AGRL | WETL | BARRL | FRST | Total |
|---|---|---|---|---|---|---|---|---|
| WATL | **27** | 0 | 0 | 0 | 0 | 0 | 0 | 27 |
| RNGB | 0 | **12** | 0 | 0 | 0 | 2 | 2 | 14 |
| URBN | 0 | 0 | **35** | 0 | 3 | 0 | 0 | 38 |
| AGRL | 0 | 0 | 0 | **29** | 9 | 6 | 0 | 44 |
| WETL | 0 | 0 | 0 | 1 | **32** | 1 | 0 | 34 |
| BARRL | 0 | 0 | 0 | 0 | 0 | **19** | 3 | 22 |
| FRST | 0 | 0 | 0 | 0 | 0 | 0 | **26** | 26 |
| Total | 27 | 12 | 35 | 31 | 44 | 31 | 31 | **203** |
| P_ accuracy (%) | 1 | 1 | 1 | 0.97 | 0.73 | 0.7 | 0.87 | |

They are diagonal cells that contain the number of correctly identified pixels (classified image) relative to ground truth samples.

Table 5: Classification accuracy and kappa statistics for various LULC maps.

| Years | Overall classification accuracy (%) | Overall kappa statistics ($k$) |
|---|---|---|
| 2000 | 0.89 | 0.87 |
| 2010 | 0.84 | 0.82 |
| 2020 | 0.85 | 0.88 |

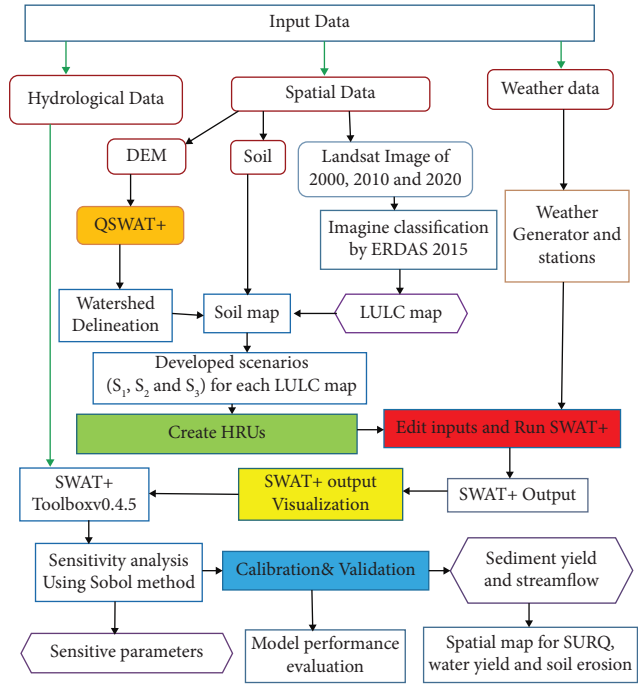


Figure 4: The overall flow diagram of the study.

$$sed = 11.8\left(Q_{Surf}\, x q_{pek}\, x area_{hru}\right) x\, K_{USLE}\, x\, C_{USLE}\, x\, P_{USLE}\, x\, LS_{USLE}\, x\, CFRG, \tag{4}$$

$$CN = \frac{\sum A_i * CN_i}{\sum A_i}, \tag{5}$$

where $A_i$ is the area (km$^2$) of the subbasin, $CN_i$ is the corresponding curve number, $Sed$ is the sediment yield (ton), $Q_{gw}$ is the surface runoff volume (mm), $q_{\text{peak}}$ is the peak runoff rate (m$^3$/s), $area_{hru}$ is the area of an HRU (km$^2$), $K_{USLE}$ is the soil erosion factor, $C_{USLE}$ is the land cover and management factor, $P_{USLE}$ is the conservation measure factor, $LS_{USLE}$ is the topographic factor, and CFRG is the coarse fragment factor [29].

*3.2. SWAT + Model Applications and Performance Criteria.* The SWAT + model is a revamped version of SWAT, which is widely used to forecast the effects of soil and land use on water resources [30]. The model interface is QGIS compatible and can integrate a wide range of geospatial data to

accurately represent watershed characteristics at the hydrological response unit (HRU) [31]. This model performs exceptionally well in simulating the effects of climate change, land use, and land cover dynamics on hydrology, streamflow, sedimentation, and groundwater [32]. The SWAT + model was used in this study to simulate land use and land cover dynamics in generating runoff and sediment yields at the HRU level in the watershed. The study also looked at the SWAT + model's ability to calibrate streamflow and sediment yields for three LULC scenarios. For these reasons, three models were created and calibrated to determine the best values of various calibration parameters for various land use maps corresponding to that climate period, as shown in Table 6.

The model's performance was evaluated by comparing the simulated output to the recorded data using statistical indicator tools such as the coefficient of determination ($R^2$), Nash–Sutcliffe model efficiency (NSE), and percentage bias (PBIAS), as shown in the following equations [33]:

$$R^2 = \frac{\sum_{i=1}^{n}(O_{i-}O_{ave})x(S_i - S_{ave})}{\left(\sum_{i=1}^{n}(O_i - O_{ave})\right)^{0.5} x \left(\sum_{i=1}^{n}(S_i - S_{ave})\right)^{0.5}}, \quad (6)$$

$$\frac{\text{BIAS} = \sum_{i=1}^{n} S_i - \sum_{i=1}^{n} O_i}{\sum_{i=1}^{n} O_i} \text{ x } 100\ \%, \quad (7)$$

$$\text{NSE} = 1 - \frac{\sum_{i=1}^{n}(O_i - S_i)^2}{\sum_{i=1}^{n}\left(O_i - \dot{O}_i\right)^2}, \quad (8)$$

where $O_i$ and $S_i$ are the observed and simulated values, $O_i$ is the mean value of the observed data, and $n$ is the total amount of the data.

*3.3. Sediment Rating Curve.* The sediment data collected from the MoWIE were insufficient for SWAT + model calibration and validation. Because the recorded data at the catchment's outlet are not time step recorded, they should be generated using Equations (9) and (10) from the plot of streamflow versus sediment [14]. Despite the fact that there were less than 10% missing data, streamflow was sufficient to calibrate and validate the model.

$$Qs = 0.0864 * Q_i * C, \quad (9)$$

where $Q_s$ is the sediment load in $t$/day, $Q_i$ is the instantaneous stream discharge in $m^3/s$ [34]. The sediment rating curve shown in Figure 5 was generated using equation (10), where a and b are constants with values of 7.9948 and 0.8218, respectively.

$$Qs = a * Qi^b. \quad (10)$$

*3.4. Calibration, Validation, and Sensitivity Analysis.* Calibration entails testing the model with known input and output data to adjust some parameters. In contrast, validation entails comparing the model results with an independent dataset without adjusting the calibration parameters further. These sensitive parameters influence runoff, percolation, lateral flow, groundwater movement to the soil, evapotranspiration, and water yields, in addition to streamflow and sediment yields. The Sobol method, Fourier amplitude, random balance design Fourier amplitude, and delta moment independent measures are the known sensitivity analysis methods in SWAT+ [35]. The Sobol method was chosen due to its widespread use in estimating significant sensitive parameters using the P-factor and the $t$-test [36]. The purpose of this calibration is to show how LULC affects runoff, soil erosion, water yield, and sediment loading in the watershed. All three models developed for land use and land cover change scenarios were calibrated using SWAT + Toolboxv0.4.5.

Table 6: Models and scenarios created in response to LULC and weather data.

| | LULC maps | Weather data |
|---|---|---|
| *Models* | | |
| $M_1$ | 2000 | 1992–2000 |
| $M_2$ | 2010 | 2003–2011 |
| $M_3$ | 2020 | 2012–2020 |
| *Scenarios* | | |
| $S_1$ | 2000 | 1992–2020 |
| $S_2$ | 2010 | 1992–2020 |
| $S_3$ | 2020 | 1992–2020 |

M: model; S: scenario.

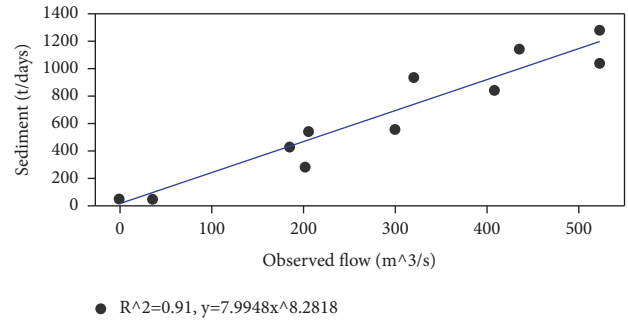


Figure 5: Sediment rating curve for the watershed.

## 4. Results and Discussion

*4.1. LULC Dynamics in the Watershed.* Significant changes in land use and land cover have occurred in the Akaki watershed since 1982. Urbanization and rising agricultural land usage are pronounced for this LULC dynamic. Numerous areas of forest and shrubland have been converted to agricultural land. Massive population shifts from rural to urban areas caused a steady change in the land cover throughout the watershed. The catchment is now exposed to heavy runoff and soil erosion, which will cause sediment loading. This rapid shift in land cover has also caused soil erosion. According to the 2002 LULC map's satellite image, 26.28% and 18.9%, respectively, of the total area were sparse forest and shrubland, as shown in Figures 6(a) and 6(b).

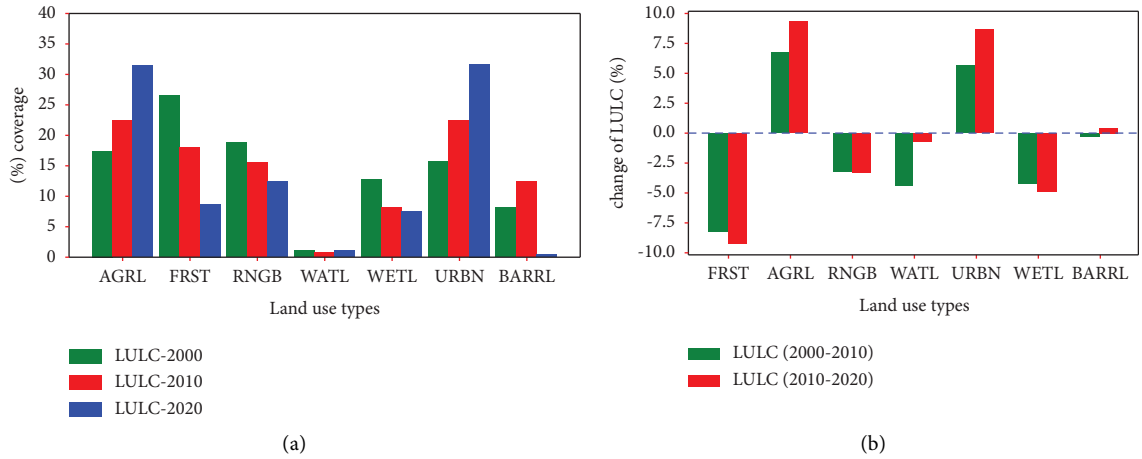


Figure 6: (a) Annual coverage in percent and (b) annual change over time in percent.

On the other hand, agriculture accounted for 15.67% of the land use that dominated the watershed and urban areas made up 17.27%. In contrast to sparse forest, which made up 17.94% of LULC in 2012, urban areas, shrubland, agricultural land, bare soils, wetland, and waterbodies made up 22.24%, 15.59%, 22.83%, 8.17%, and 0.84% of the total area, respectively. Sparse forest, shrubland, and wetlands were decreasing among the existing LULC, with 8.86%, 3.2%, and 4.55%, in the first ten years, respectively. Urban areas, agricultural land, and bare soils are three other LULC modifications that are increasing by 6.57%, 5.56%, and 4.29%, respectively. The annual LULC change is generally examined with substantial deforestation for agriculture and urbanization for settlements over the study period for the past twenty years. Under these circumstances, annual forest removal has been 9.3%, while urban and agricultural lands have taken up 4.4% and 4% of the total area, respectively, as shown in Table 7.

*4.2. Performance of the SWAT+ Model during Streamflow Calibration and Validation.* Calibration prioritizes ten sensitive parameters that affect streamflow simulations based on the recorded flow at the watershed's outlet for each period. As shown in Table 8, the most sensitive parameters were selected as the curve number (**Cn2**), **cn3_swf**, soil evaporation compensation factor (**esco**), plant uptake compensation factor (**epco**), soil layer available water capacity (**sol_awc**), and baseflow alpha factor (**alpha_bnk**). **flo_min**, **revap.co**, and **usle_k** were the other parameters in the second division of sensitive parameters with medium influences on surface runoff and baseflow.

The remaining parameters are designated as less sensitive. The periodical calibrated streamflow with a good SWAT+ performance is based on the selected performance criteria and the model output with the scenario ($S_1$). The average values of $R^2 = 0.88$, **NSE** = 0.9, and **PBIAS** = −2.36 indicate that the model is well-suited for simulating flow. The P-factors and R-factors with well-fitted values were used to evaluate the goodness of fit and the degree to which the SWAT + model's calibrated streamflow. The calibration and validation results of streamflow for three scenarios are presented separately in Figures 7(a) and 7(b), with good agreement against the observed data. This demonstrates how the SWAT+ model is effective, reliable, and efficient in simulating hydrological processes at the HRU level under surface and subsurface conditions.

*4.3. Sediment Yield Calibration and Validation.* The simulated sediment yield was calibrated against the observed data and prioritized nine sensitive parameters that affect sediment yields at the subwatershed. The most sensitive parameters were identified as USLE support practice factors (**Usle_p**), USLE soil erodibility factors (**uslek_lte**), sediment intensity in LAT and GW (**lat_sed.hru**), re-entrained channel sediment routing (**spex.bsn**), the parameter for channel sediment routing (**SP.con.bsn**), and channel erodibility factors (**ch.cov2.rte**). The calibrated values of each sensitive parameter listed in Table 9 show that the model was fit to simulate sediment yields in the catchments compared to the recorded ones. The other remaining parameters were sensitive but not as sensitive as the first five selected. The performance of the SWAT+ model was measured using average statistical tool values, with $R^2 = 0.82$, **NSE** = 0.86, and **PBIAS** = 4.38 which show strong numerical agreement, as depicted in Figures 8(a) and 8(b).

*4.4. The Effect of Changing LULC on Runoff, Sediment Yields, and Water Yields.* With a total area of 1187 km$^2$, the watershed has been divided into twelve subwatersheds based on different drainage patterns of the land surface terrain. $SW_1$, $SW_2$, $SW_3$, $SW_4$, $SW_{10}$, $SW_{11}$, and $SW_{12}$ are the most common subwatersheds in the upper parts of the watershed, with an average elevation of 2705 m to 3380 m. In these subwatersheds, surface runoff, soil erosion, and water yields are three of the most prevalent hydrological processes that are influenced by the variety of land cover, slope, and soils. The watershed contains 22,993 HRUs and 267 LSUs. Each hydrological response unit comprises various land uses and land covers, hydrological soil groups, and slopes.

Table 7: LULC change and the rate of change comparisons for 2000, 2010, and 2020.

| LULC classes | 2000 | | 2010 | | 2020 | | Change (%) | | Rate of change (%) | |
|---|---|---|---|---|---|---|---|---|---|---|
| | Area ($km^2$) | % | Area ($km^2$) | % | Area ($km^2$) | % | (2000–2010) | (2010–2020) | (2000–2010) | (2010–2020) |
| FRST | 312 | 26.3 | 213 | 17.9 | 103 | 8.7 | −8.3 | −9.3 | −3.8 | −9.1 |
| URBN | 186 | 15.7 | 264 | 22.2 | 374 | 31.5 | 6.6 | 9.3 | 3.5 | 4.4 |
| RNGB | 223 | 18.8 | 185 | 15.6 | 146 | 12.3 | −3.2 | −3.3 | −1.9 | −3.0 |
| WETL | 151 | 12.7 | 97 | 8.2 | 89 | 7.5 | −4.5 | −0.7 | −4.4 | −1.1 |
| AGRL | 205 | 17.3 | 271 | 22.8 | 373 | 31.4 | 5.6 | 8.6 | 2.8 | 4.0 |
| BARRL | 96 | 8.1 | 147 | 12.4 | 89 | 7.5 | 4.3 | −4.9 | 4.3 | −6.3 |
| WATL | 14 | 1.2 | 10 | 0.8 | 13 | 1.10 | −0.3 | 0.3 | −3.4 | 3.3 |

Table 8: With developed models, the best calibration parameters and their fitted values.

| Rank | Name | OBJ types | ABS_Min | ABS_Max | Model-calibrated values | | |
|---|---|---|---|---|---|---|---|
| | | | | | $M_1$ | $M_2$ | $M_3$ |
| 1 | cn2 | hru | 35 | 95 | 63 | 72 | 88 |
| 2 | cn3_swf | hru | 0 | 1 | 0.94 | 0.87 | 0.96 |
| 3 | awc | sol | 0.01 | 1 | 0.84 | 0.72 | 0.86 |
| 4 | esco | hru | 0 | 1 | 0.56 | 0.74 | 1 |
| 5 | epco | hru | 0 | 1 | 0.78 | 0.86 | 0.97 |
| 6 | alpha | aqu | 0 | 1 | 1 | 0.65 | 0.72 |
| 7 | revap_min | aqu | 0 | 50 | 28 | 35 | 41 |
| 8 | revap-co | aqu | 0.02 | 0.2 | 0.13 | 0.14 | 0.16 |
| 9 | usle_k | sol | 0 | 0.65 | 0.48 | 0.57 | 0.65 |
| 10 | Flo_min | sol | 0 | 30 | 21 | 19 | 26 |

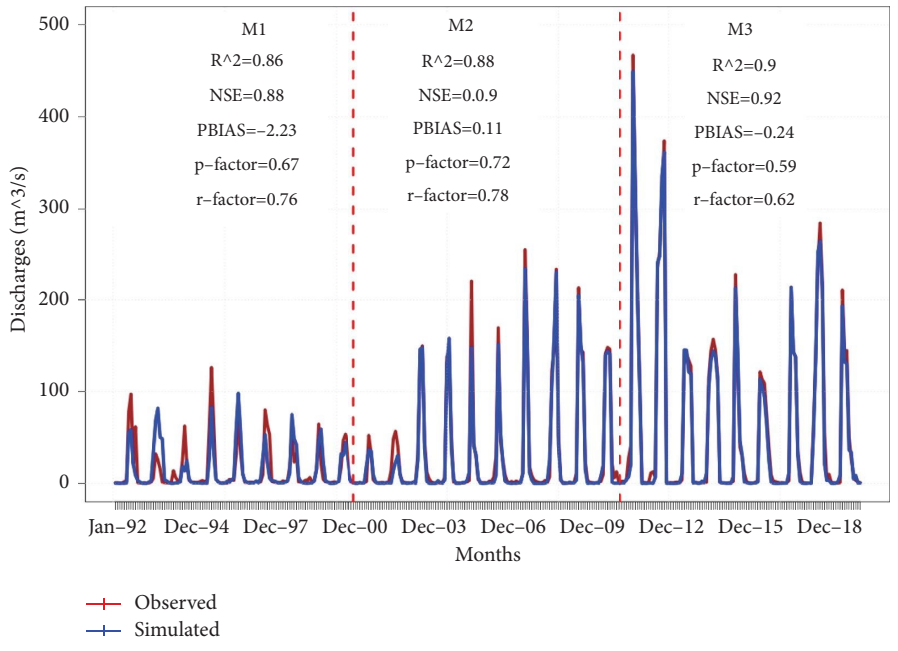


(a)

Figure 7: Continued.

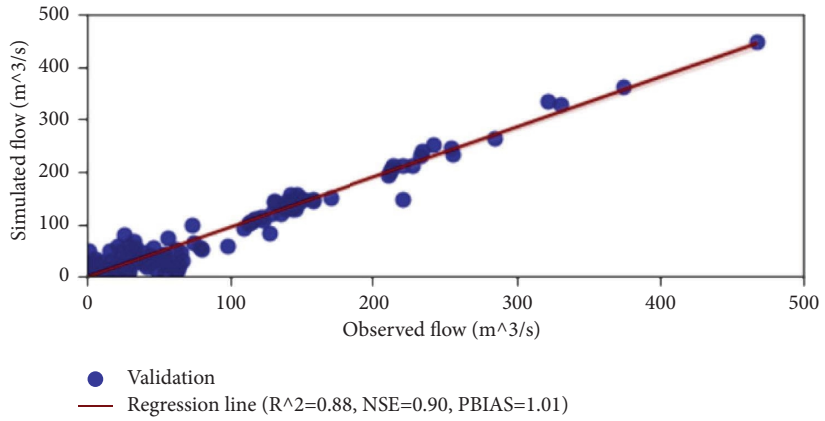


(b)

Figure 7: Streamflow calibration (a) and validation (b) for three consecutive scenarios.

Table 9: The calibrated values of sensitive parameters.

| Rank | Name | Object | Description | Min | Calibrated | Max |
|---|---|---|---|---|---|---|
| 1 | Usle_p | hru | USLE support practice factor | 0 | 0.72 | 1 |
| 2 | uslek_lte | hlt | USLE soil erodibility factors | 0 | 0.482 | 0.65 |
| 3 | Lat_sed.hru | hru | Sediment intensity in LAT and GW | 0 | 64 | 120 |
| 4 | spex.bsn | bsn | Re-entrained channel sediment routing | 1 | 1.134 | 2 |
| 5 | SP.con.bsn | bsn | Parameter for channel sediment routing | 0 | 0.0028 | 0.01 |
| 6 | ch_cov2.rte | rte | Channel erodibility factors | 0.6 | 0.88 | 1 |
| 7 | ch_eqn.rte | rte | Sediment routing method | 0 | 0.00065 | 0.001 |
| 8 | Slope_k | hru | Slope intensity at hru | 0 | 0.76 | 0.9 |
| 9 | Surlags | bsn | Sediment concentration lag time | 0.05 | 13.4 | 24 |

The output of the SWAT+ model is dependent on the discretized subwatershed to HRUs rather than the subbasin, as was well known in the previous version of SWAT. Three models ($M_1$, $M_2$, and $M_3$) were developed for each scenario with the same number of HRUs in the watershed region, assuming that DEM, soil maps, and climate variables remain constant and dynamic in LULC for three decades. Surface runoff, soil erosion, and water yields were increased from $S_1$ to $S_3$ for an average annual precipitation of 1938.05 mm.

The rapidly expanding agricultural area and deforestation result in the potential for increased surface runoff, soil erosion, and water yields. Lower infiltration rates and higher surface runoff specifically followed the expansion of urban areas. Water yields increased from $S_1$ to $S_2$ by 22.2% and from $S_2$ to $S_3$ by 33.25%. Surface runoff rose from $S$ to $S_2$ by 37.04% and from $S_2$ to $S_3$ by 42.7%. Table 10 shows that sediment yields increased by 52.5% from $S_1$ to $S_2$ by 52.5% and from $S_2$ to $S_3$ by 58.34%. This suggests that the sediment yield is increasing over time due to land cover variability. Furthermore, changes in land use and land cover also raise the curve number values. This trend indicates that the increasing average curve number values for the antecedent of soil moisture-II (cn2) result in increased surface runoff. The developed spatial map for surface runoff, water yields, and sediment yields for annual rainfall distributions shows that urban areas were the most vulnerable to surface runoff, water yields, and sediment loading for the LULC of 2000. For the dynamic land cover, the spatial map represents a linear relationship between surface runoff and the curve number, as well as the water yield.

*4.5. Exceedance Probability of the Runoff Relationship between Water Yields and Sediment Yields.* The statistical data demonstrate that the variation in LULC continuously modifies the amount of surface runoff, water yields, and sediment loads. The analysis shows the degree to which each component is influenced by LULC changes and the probability that each component will exceed its annual probability in the future. According to the flood hydrograph exceedance probability plotted in Figure 9, there was a less than 9.8% chance of rainfall at each station, exceeding annual maximum records. In terms of surface runoff, there was a less than 20% chance of a new annual runoff magnitude being recorded between 2000 and 2020 that exceeded the highest simulated magnitude. This demonstrates how rainfall and surface runoff are closely related to these catchments. However, the probability of annual exceedance is greater than 60% for annual surface runoff, water yields, and sediment yields. This influence has been expected from marginalized impacts of both climate change and land use dynamics. However, the exceedance probability of water yields to altering the simulated maximum value with each scenario was more than 65% in the last two decades.

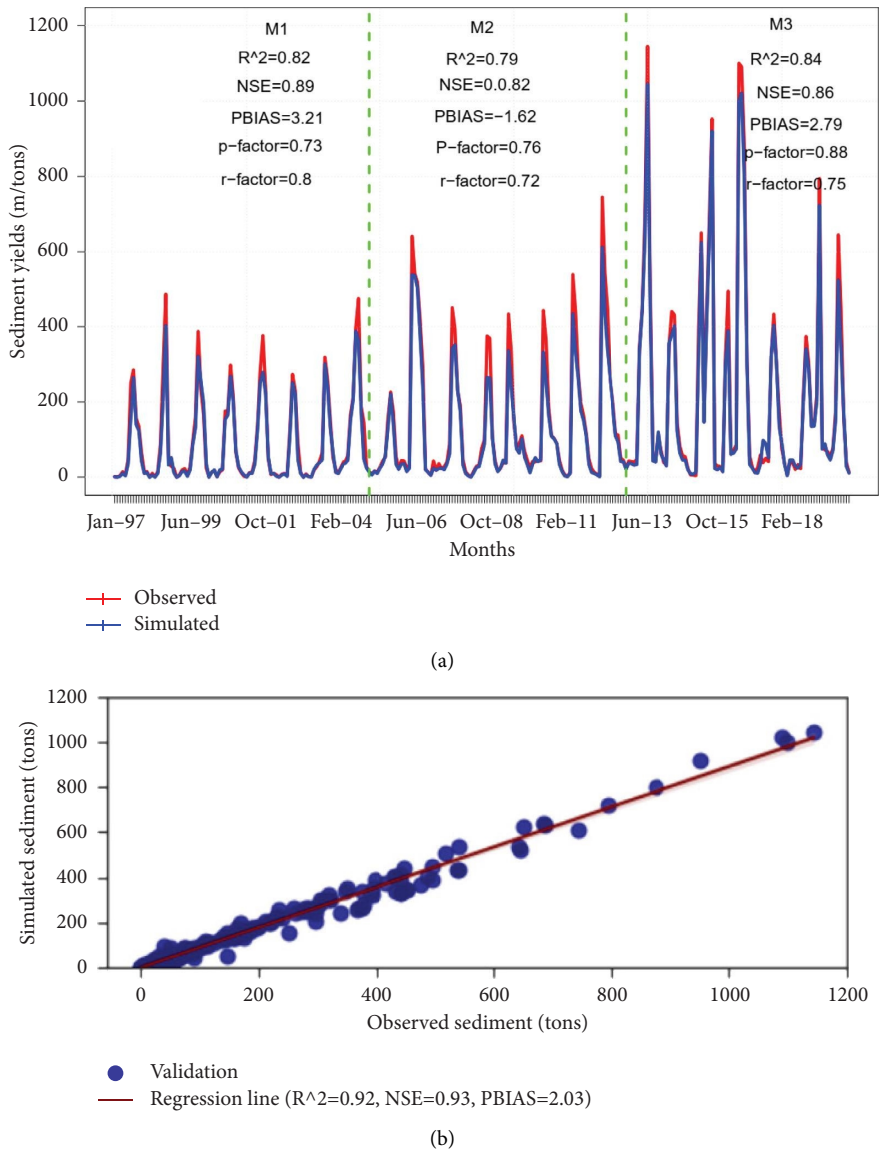


Figure 8: Calibration (a) and validation (b) of sediment yields for three scenarios.

Moreover, surface runoff and water yields were showing an increasing trend along with the changes in LULC. Generally, the annual exceedance probability reveals the significant relationship between LULC changes and surface runoff and sediment yields. According to this study, the responses of various LLCs to runoff, sediment yields, and significant hydrological processes varied by more than 70%. Hence, the best land use management in this watershed with effective implementation can reduce the impacts of land use change on initiating surface runoff, soil erosion, and sediment yields.

*4.6. Potential Runoff and Water Yield Contributing Areas at the Subwatershed Level.* A large LULC change has occurred in the Akaki watershed, which comprises two catchments with different land use and land cover distributions. Each LULC has its own effect on accelerating runoff and sediment yields in catchments through mass soil erosion. Agriculture and bare soils, which cause soil erosion, are the most vulnerable land uses in this watershed. Urban areas and bare soil, which have lower infiltration rates, contribute a large amount of surface runoff to channels. The simulated flood hygrograph of the main channel shows that the expansion of urban areas has taken advantage of increased surface runoff more than any other LULC. Since 2000, agricultural land has covered most eastern and western parts of the watershed, and this trend also continues as urbanization takes over. Agricultural land practices have partially covered the western portions of the Akaki watershed, making up 22.83% of the total area, according to a LULC-classified satellite image from 2010. Agricultural areas in the western portions of these catchments started to decline after ten years and were gradually turned into urban areas by 2020. However, the eastern parts of the watershed, which were previously covered by forest and wetland, were converted to agriculture

Table 10: SURQ, water yield, CN values, and sediment yield as a function of the model.

| Scenarios | Rainfall (mm) | Runoff (mm) | Water yield (mm) | Sediment yield (t/ha) | CN |
|---|---|---|---|---|---|
| $S_1$ | 1938.05 | 66.58 | 186.2 | 241.8 | 66.64 |
| $S_2$ | 1938.05 | 210 | 232.5 | 408.7 | 72 |
| $S_3$ | 1938.05 | 322 | 324.2 | 732.4 | 88 |

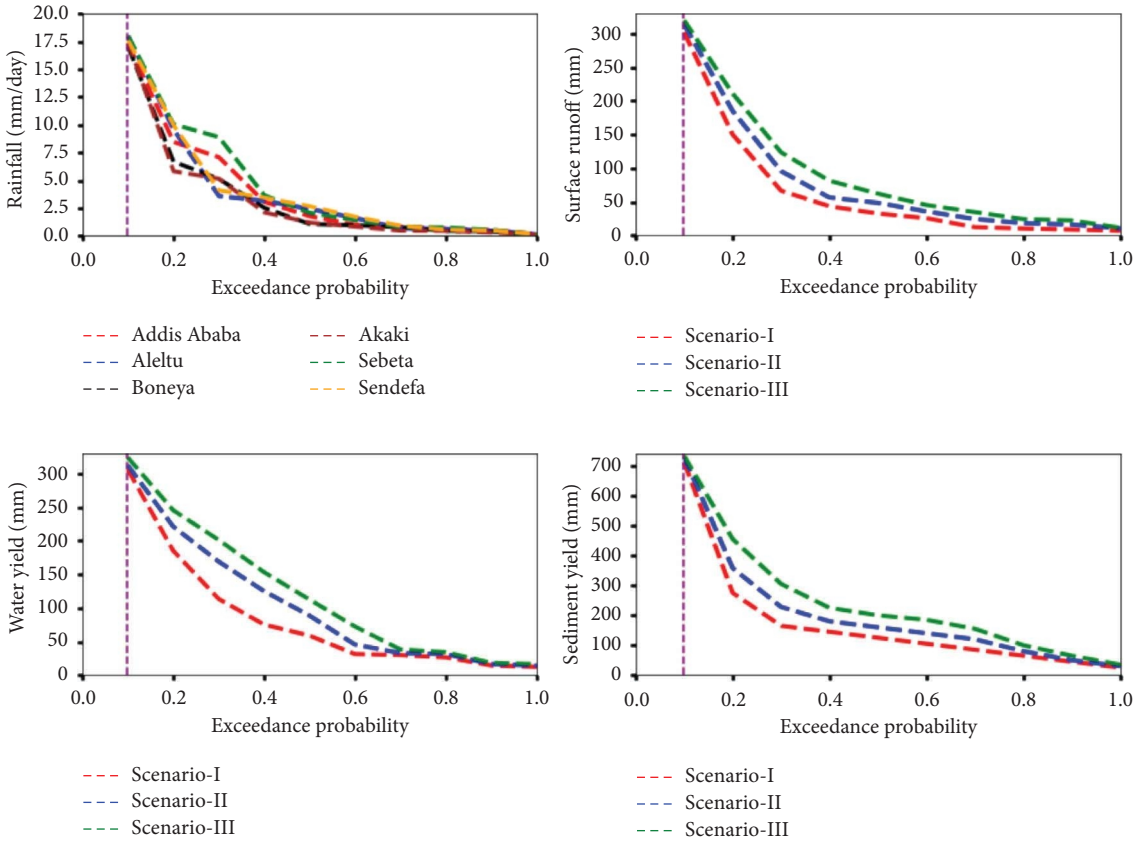


Figure 9: Annual exceedance probability of runoff and sediment yields under LULC changes.

and increased by 31.42%. Because of the rapid change in land use and cover, the status of surface runoff and sediment yields has increased at the subwatershed level from decade to decade.

The spatial map created for LULC 2020, which includes the mean annual distributions of surface runoff and water yields, illustrates how these hydrological processes are developing in relation to land cover variability, as shown in Figure 10. The calibrated results using various LLCs show that soil erosion, surface runoff, and sediment yields have increased in this watershed. In the three developed models, the proportional contribution of each individual LULC to surface runoff and sediment yields varied depending on the developed scenario. The findings show that agricultural land and bare soils are the primary contributors to surface runoff and sediment yields, followed by built-up areas, which significantly contribute to surface runoff but very little to sediment yields compared to runoff.

*4.7. Annual Sediment Yield at Subwatersheds under Each Scenario.* For each scenario, the model calculated annual sediment yields with mean values of 241.8 tons/ha, 408.7 tons/ha, and 732.4 tons/ha, which indicate strong increasing trends. This value shows that there is a significant risk of rising sediment bed levels due to the rapid growth in the amount of sediment yield produced by the watershed and loading into the reservoir. The most sensitive subwatersheds that generated sediment yields were $SW_1$, $SW_3$, $SW_4$, and $SW_{10}$, which had high sediment deposition during the calibration with LULC in 2000, 2010, and 2020. The subwatershed settings and highly elevated topography increased their susceptibility to sedimentation.

Conversely, $SW_2$, $SW_6$, $SW_7$, $SW_9$, and $SW_{12}$ contributed the least amount of sediment yields to channels that deliver to the watershed's downstream parts, with annual mean values of 264.5tons/ha. The remaining subwatersheds contribute a moderate amount of sediment. In all scenarios

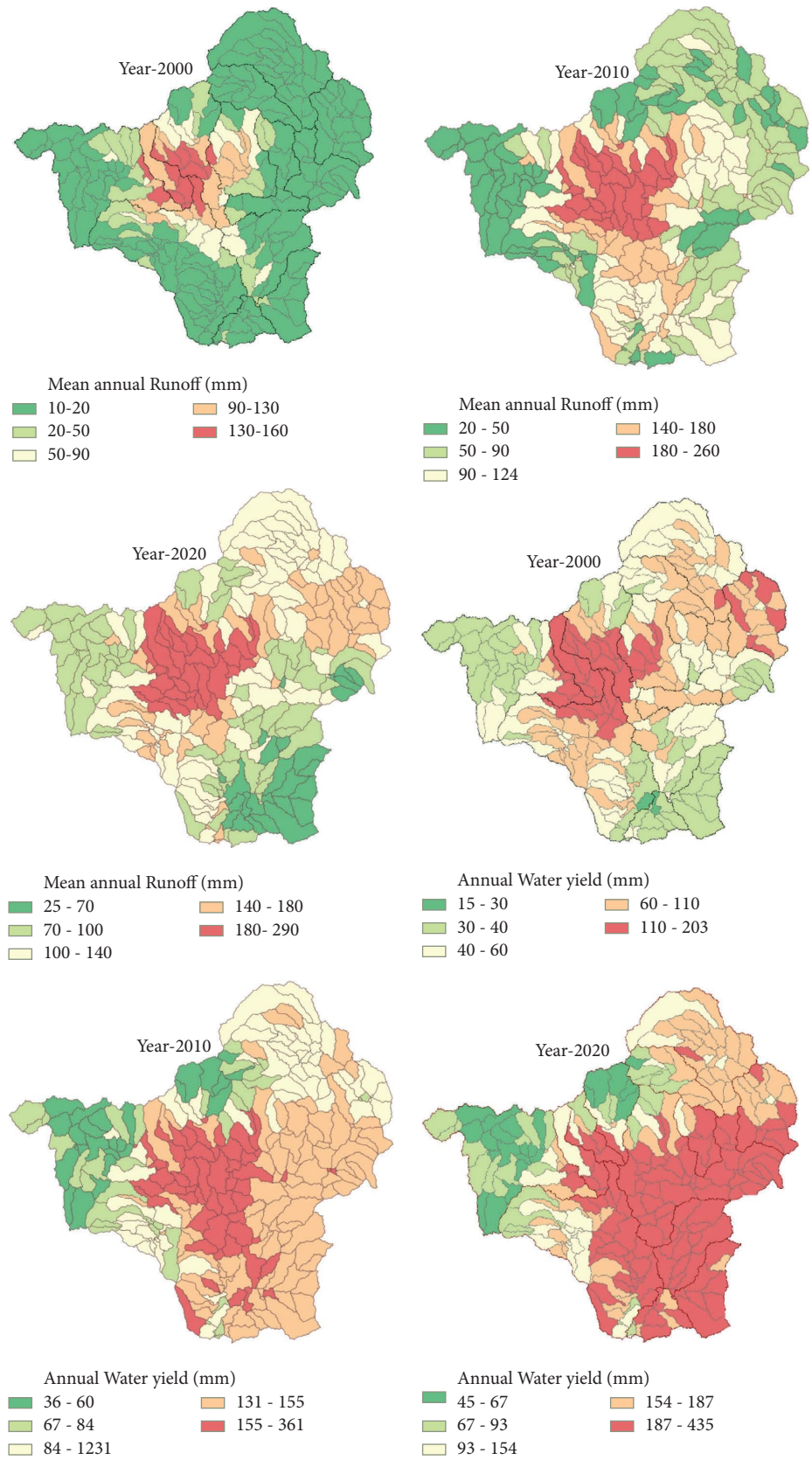


Figure 10: Spatial maps of potential runoff and water yields at LSUs in the catchment.

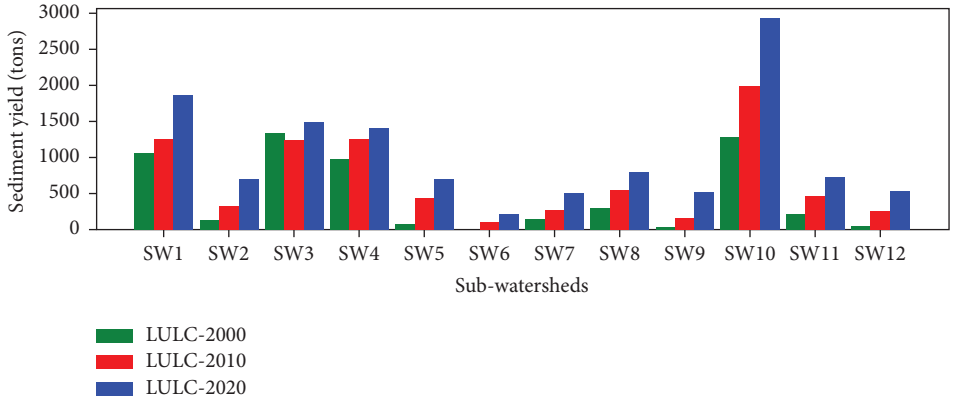


Figure 11: Sediment yields at the subwatershed level for LULC from 2000 to 2020.

of land use and land cover, with increasing sediment yields in the reservoir, the majority of subwatersheds were subject to soil erosion. Agricultural land has been heavily converted to urban areas in two subwatersheds, $SW_1$ and $SW_{11}$, while forest and shrubland have been partially converted to urban and agricultural land uses.

The hydrological processes of the watershed changed as a result of the quick change in land cover. In these cases, annual increases in surface runoff and sediment yields were reported. On the other hand, the SWAT+ model does not calculate or simulate hydrological processes at the subbasin level. With multiple landscape units (LSUs), streamflow and sediment yields are stimulated and calibrated at the subwatershed level.

The sediment released from each landscape unit into the watershed is measured and depicted in Figure 11 at the subbasin outlet. The annual output of the upland sediment yield shows that, in 2000, 2010, and 2020, respectively, 7.5%, 8.23%, and 12.1% of the watershed sediment load were generated from each subwatershed region due to the LULC change. The erodibility of the channels was 25%, 14.2%, and 18% with respect to each of the LULC scenarios, as shown in Table 11.

*4.8. Sediment Yield Hotspot Areas at Subwatershed Levels.* The spatial variability of sediment yields in the catchment identifies regions with high rates of soil erosion as a result of changes in land use and land cover. The combined effects of LULC changes, soil types, climate change, and rising runoff have resulted in an increase in sediment yields. In order to identify the most severe area of the catchment and recommend appropriate mitigation measures, this study used the annual average value of sediment yields to create a spatial variability map of sediment concentration from each landscape unit. Based on the defined number of landscape units as shown in Figure 12**,** the spatial map was created to identify various sediment yield-prone areas. According to this severity class, 182 LSUs were designated as low-vulnerable areas to soil erosion, and only one LSU was highly exposed to sediment yields as a result of soil erosion in the first scenario. Bare soil, shrubland, and some areas of the urban area covered the majority of the landscape units that

Table 11: Streamflow and sediment budget components and their variation under LULC changes.

| Streamflow and sediment budget | Scenarios' | | |
|---|---|---|---|
| | $S_1$ | $S_2$ | $S_3$ |
| Upland sediment yield (%) | 7.5 | 8.23 | 12.1 |
| Instream sediment yields (%) | 42.5 | 38.4 | 62.4 |
| Total streamflow losses (%) | 7.8 | 16.3 | 12.6 |
| Seepage losses (%) | 3.24 | 10.8 | 16.25 |
| Channel erosion (%) | 25 | 14.2 | 18 |

were highly susceptible to soil erosion. It is located in the center of both catchments and has a 15.1 ha vulnerable area, with a total annual sediment yield of 31.14 tons. On the other hand, the majority of the soil erosion-prone regions that were classified as severe in the second and third scenarios covered a sizable area of urban, agricultural, and shrubland. These soil erosion hotspots covered an area of 3,777.3 ha (3.18%) and 13,413.1 ha (11.3%), with a total annual sediment yield of 361.93 m/tons and 1239.24 m/tons, respectively, as depicted in Table 12. In the lower reaches of the catchment, soil types like luvisols, leptosols, and Cambisols with steep slopes were justified as the most susceptible to soil erosion. Some areas of the catchment in the downstream part show a decreasing pattern from very high sediment yield to high as a result of land recovery, because the area was covered by agriculture in the 2010s and later partially covered by wetlands and sparse forests. This change in land use in the 2020s has resulted in a decrease in sediment yields as a result of decreasing floods compared to 2010. In general, the developed scenario demonstrates how LULC changes have accelerated soil erosion due to high flooding, leading to increased sediment yields at catchment downstream.

*4.9. The Impacts of Each Land Use and Land Cover on Runoff and Sediment Yields.* The results reveal that the hydrological response of the catchments is significantly impacted by changes in land use and land cover from $S_1$ to $S_3$, as shown in Table 13**.** The increases in sediment yields and surface runoff, as well as decreases in baseflow and lateral flow, were all closely correlated with changes in land use and land cover.

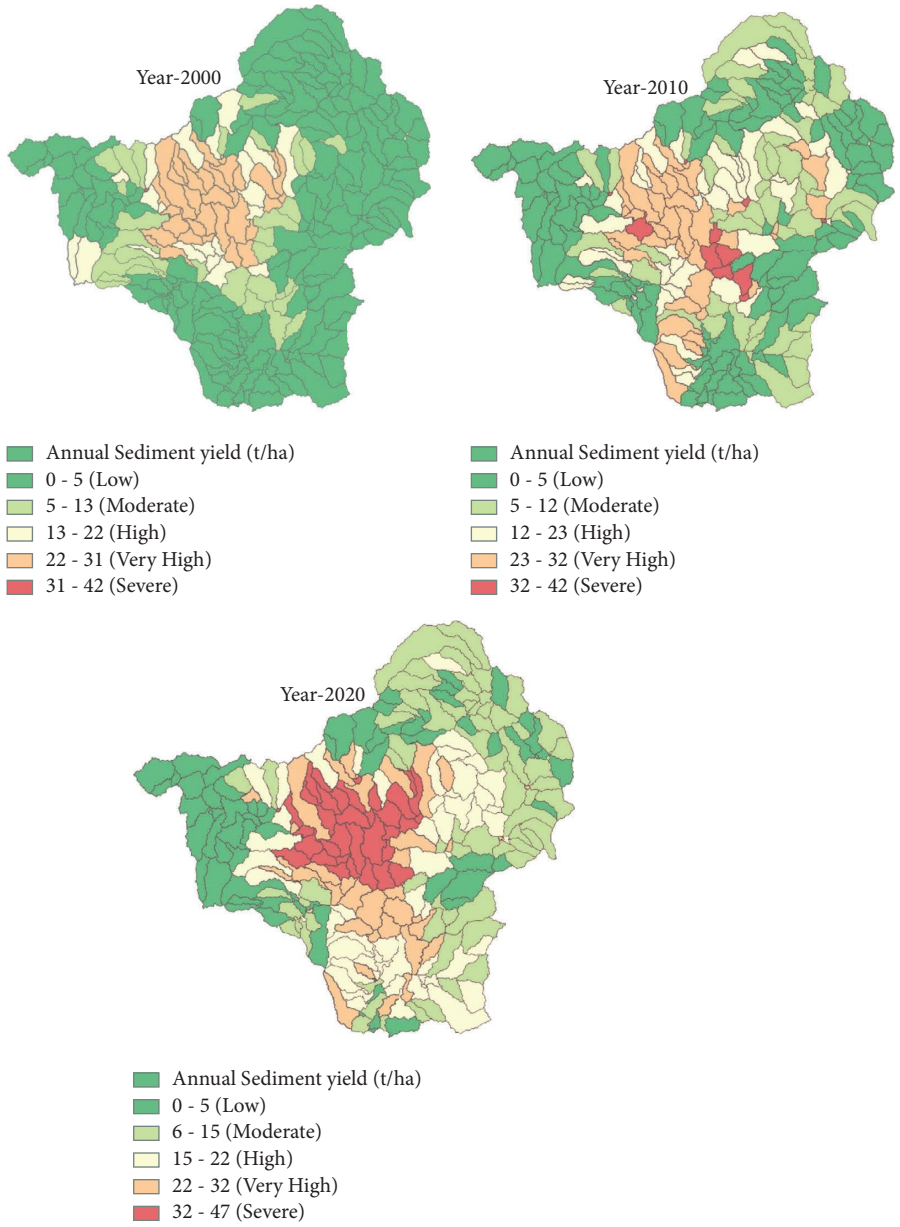


Figure 12: Spatial map of soil erosion-prone LSUs at subwatershed levels.

Table 12: Soil erosion-prone landscape units (LSUs) in the watershed with sediment yield (t/ha).

| $S_1$ | | | $S_2$ | | | $S_3$ | | |
|---|---|---|---|---|---|---|---|---|
| LSUs ID | Area (ha) | Sediment yield (t/ha) | LSUs ID | Area (ha) | Sediment yield (t/ha) | LSUs ID | Area (ha) | Sediment yield (t/ha) |
| 1020 | 15.1 | 31 | 110 | 70.2 | 30.4 | 140 | 95 | 33.7 |
| | | | 120 | 356 | 32.5 | 170 | 670 | 35.2 |
| | | | 130 | 95 | 30.12 | 320 | 482 | 44.23 |
| | | | 170 | 670 | 35.2 | 340 | 156 | 32.4 |
| | | | 280 | 656 | 42.8 | 380 | 240 | 34.2 |
| | | | 390 | 637 | 33.41 | 390 | 228 | 36.2 |
| | | | 450 | 216 | 31.41 | 450 | 216 | 33.1 |
| | | | 730 | 611 | 32.5 | 540 | 1258 | 45.2 |
| | | | 1020 | 15.1 | 30.05 | 550 | 472 | 38.41 |
| | | | 1810 | 212 | 30.14 | 590 | 1051 | 43.7 |
| | | | 1850 | 239 | 33.4 | 640 | 352 | 35.8 |

Table 12: Continued.

| $S_1$ | | | $S_2$ | | | $S_3$ | | |
|---|---|---|---|---|---|---|---|---|
| LSUs ID | Area (ha) | Sediment yield (t/ha) | LSUs ID | Area (ha) | Sediment yield (t/ha) | LSUs ID | Area (ha) | Sediment yield (t/ha) |
| | | | | | | 730 | 611 | 41.3 |
| | | | | | | 800 | 233 | 30.2 |
| | | | | | | 820 | 431 | 40.8 |
| | | | | | | 860 | 425 | 36.2 |
| | | | | | | 890 | 391 | 34.3 |
| | | | | | | 1020 | 15.1 | 31.14 |
| | | | | | | 1090 | 322 | 32.5 |
| | | | | | | 1210 | 147 | 31.2 |
| | | | | | | 1240 | 569 | 41.91 |
| | | | | | | 1270 | 380 | 37.4 |
| | | | | | | 1810 | 212 | 32.2 |
| | | | | | | 1900 | 261 | 39.41 |
| | | | | | | 1930 | 228 | 30.23 |
| | | | | | | 1960 | 678 | 42.3 |
| | | | | | | 1980 | 511 | 45.2 |
| | | | | | | 2030 | 646 | 38.4 |
| | | | | | | 2050 | 395 | 34.2 |
| | | | | | | 2060 | 278 | 32.8 |
| | | | | | | 2170 | 368 | 33.6 |
| | | | | | | 2200 | 293 | 43.37 |
| | | | | | | 2230 | 232 | 31.2 |
| | | | | | | 2290 | 235 | 34.04 |
| | | | | | | 2300 | 332 | 33.2 |

Table 13: Contribution of each LULC to cause surface runoff, water yield, and sediment yield.

| LULC classes | Scenario I | | | Scenario II | | | Scenario III | | |
|---|---|---|---|---|---|---|---|---|---|
| | SURQ (mm) | SED (T/ha) | WYLD (mm) | SURQ (mm) | SED (T/ha) | WYLD (mm) | SURQ (mm) | SED (T/ha) | WYLD (mm) |
| Forest | 10.1 | 2.7 | 42.3 | 13.53 | 28.34 | 62.1 | 34.1 | 48.2 | 78.3 |
| Urban | 132 | 53.1 | 186.2 | 177.04 | 101.6 | 201.2 | 246.1 | 167.3 | 345.2 |
| Shrubland | 23.4 | 64.2 | 39.6 | 53.78 | 97.2 | 68.1 | 93.1 | 191.2 | 93.1 |
| Agriculture | 19.8 | 11.6 | 73.2 | 38.5 | 25.36 | 81.3 | 57.4 | 117.4 | 142.1 |
| Wetland | 6.84 | 1.15 | 8.73 | 11.8 | 1.25 | 17.02 | 10.12 | 1.18 | 15.7 |
| Bare soils | 21.9 | 110.2 | 32.1 | 42.43 | 156.2 | 59.3 | 75.2 | 208.3 | 86.3 |

SURQ: surface runoff (mm); SED: sediment yield (t/ha); WYLD: water yield (mm); CN: curve number.

Rapidly increasing runoff generation, water yields, and sediment yields with decreasing baseflow have an impact on sustenance flow regimes, particularly during the dry season flows. An increased runoff of 10.12 mm to 13.53 mm and 13.53 mm to 34.1 mm from $S_1$ to $S_3$ was correlated with the conversion of forests to agriculture. The increase in storm runoff is primarily caused by a decrease in the infiltration rate when forests are converted to other land uses.

On the other hand, the increased water yield and surface runoff in the catchment result in environmental problems like soil erosion and water body sedimentation. Due to growing urbanization and declining forest density, surface runoff has increased by 2.9% to 9.24% from $S_1$ to $S_2$ and $S_2$ to $S_3$, respectively. On the other hand, water yields have increased by 3.84% to 2.32%, and sediment yields have increased by 4.99% to 6.52% from $S_1$ to $S_2$ and $S_2$ to $S_3$, respectively. In general, the loss of forest land causes an open surface, which creates an opportunity for soil erosion, which results in sediment yields at the outlet. In addition, the growth of urban areas and bare soil has contributed to an increase in surface runoff and water yields as a result of a decline in the infiltration rate. In conclusion, the watershed has experienced significant changes in land use and land cover over the past two decades, which have increased surface runoff, water yields, and sediment yields. However, this LULC modification also affects other hydrological processes like evapotranspiration, groundwater recharges, lateral flow, and percolation, as shown in Figure 13.

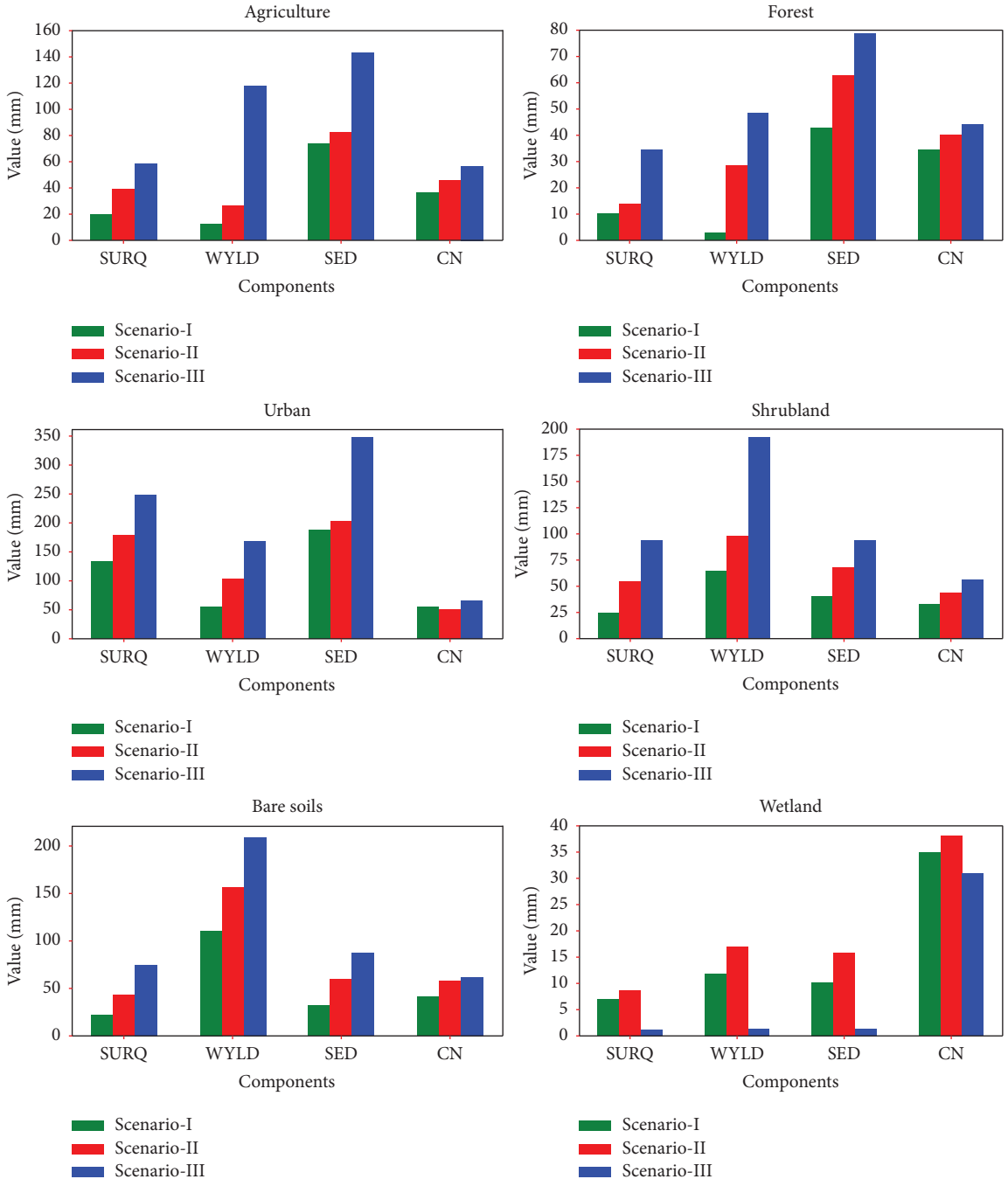


Figure 13: The contribution of each LULC to cause surface runoff, water yields, and sediment yields.

## 5. Conclusions

The land use and land cover changes in semihumid and subtropical watersheds have had a significant impact on surface runoff, sediment yields, soil erosion, and water yields. The change in the LULC has changed the ratio of the hydrological components and the ecological system. The trend of hydrological processes simulated by the SWAT + model showed an increase in both surface runoff and sediment loads. This increased sediment yield was primarily caused by soil erosion from the watershed's uplands as a result of increasing floods. The findings revealed that the majority of the LULC changes causing runoff in this watershed were caused by an increase in urban, bare soils, and agricultural land. Meanwhile, conversion of forest and shrubland to other land uses increases the likelihood of flooding caused by runoff. Furthermore, the study evidently shows that the number of LSUs exposed to soil erosion-prone areas increased from $S_1$ to $S_3$. The SWAT + model calibrated streamflow and sediment with good agreement, as indicated by statistical parameter values of $R^2 = 0.88$, NSE = 0.9, and PBIAS = 2.36; $R^2 = 0.82$, NSE = 0.86, and PBIAS = 4.38; $R^2 = 0.88$, NSE = 0.91, and PBIAS = 1.01; and

$R^2 = 0.92$, NSE = 0.93, and PBIAS = 2.03 for calibration and validation, respectively.

The conclusions are drawn as follows:

(i) The study shows that the increase of urbanization by 6.6% in 2010 and 9.3% in 2020 and that of agricultural land by 5.6% by 2010 and 8.6% by 2020 in the subbasin paves the way for the increment of surface runoff and sediment yields in three scenarios. Thus, agricultural land expansion leads to the increasing rate of soil erosion in most western and eastern parts of the watershed.

(ii) The occurrence of surface runoff in all parts of the watershed causes high flooding which instigates soil erosion. The conversions of forest and shrubland to agriculture increase soil erosion due to increasing runoff.

(iii) In addition, the decrease of forest land by 8.3% in 2010 and 9.3% in 2020 increased soil erosion, runoff, and sedimentation.

(iv) Huge masses of sediment yields and surface runoff were simulated from agricultural land and bare soils. This is due to bare soil being very sensitive to flooding and noted as the most susceptible LULC to soil erosion and surface runoff in this study.

(v) In simulating and predicting hydrological processes at HRUs rather than sub-basins, the new model is more efficient, flexible, and effective than the previous version.

## Data Availability

All necessary data were included in the paper.

## Conflicts of Interest

The author declares that there are no conflicts of interest.

## Acknowledgments

The author would like to thank all those who helped them for the successful completion of the research.

## References

[1] M. Kidane, A. Bezie, N. Kesete, and T. Tolessa, "The impact of land use and land cover (LULC) dynamics on soil erosion and sediment yield in Ethiopia," *Heliyon*, vol. 5, no. 12, Article ID e02981, 2019.

[2] T. Belay and D. A. Mengistu, "Remote sensing applications: society and environment land use and land cover dynamics and drivers in the muga watershed , upper Blue nile basin , Ethiopia," *Remote Sensing Applications: Society and Environment*, vol. 15, Article ID 100249, 2019.

[3] M. Mohammadi, A. Khaledi Darvishan, V. Spalevic, B. Dudic, and P. Billi, "Analysis of the impact of land use changes on soil erosion intensity and sediment yield using the intero model in the talar watershed of Iran," *Water (Switzerland)*, vol. 13, no. 6, p. 15, 2021.

[4] K. Solaimani, S. Modallaldoust, and S. Lotfi, "Investigation of land use changes on soil erosion process using geographical information system," *International journal of Environmental Science and Technology*, vol. 6, no. 3, pp. 415–424, 2009.

[5] W. T. Dibaba, T. A. Demissie, and K. Miegel, "Drivers and implications of land use/land cover dynamics in Finchaa Catchment, Northwestern Ethiopia," *Land*, vol. 9, no. 4, pp. 113–122, 2020.

[6] M. B. Moisa, D. A. Negash, B. B. Merga, and D. O Gemeda, "Impact of land-use and land-cover change on soil erosion using the RUSLE model and the geographic information system: a case of Temeji watershed, Western Ethiopia," *Journal of Water and Climate Change*, vol. 12, no. 7, pp. 3404–3420, 2021.

[7] T. Gashaw, T. Tulu, M. Argaw, and A. W. Worqlul, "Modeling the impacts of land use–land cover changes on soil erosion and sediment yield in the Andassa watershed, upper Blue Nile basin, Ethiopia," *Environmental Earth Sciences*, vol. 78, no. 24, 2019.

[8] G. T. Ayele, A Kuriqi, M. A Jemberrie, and S. M Saia, "Sediment yield and reservoir sedimentation in highly dynamic watersheds: the case of koga reservoir, Ethiopia," *Water*, vol. 13, 2021.

[9] M. Bayisa and D. Adeba, "Land use land cover dynamics on sediment yield modeling of angar sub-basin , Blue nile basin," *Ethiopia*, vol. 10, no. 4, pp. 62–74, 2021.

[10] G. D. Betrie, Y. A. Mohamed, A. Van Griensven, and R. Srinivasan, "Sediment management modelling in the Blue Nile Basin using SWAT model," *Hydrology and Earth System Sciences*, vol. 15, pp. 807–818, 2011.

[11] P. Munoth and R. Goyal, "Impacts of land use land cover change on runoff and sediment yield of Upper Tapi River Sub-Basin," *International Journal of River Basin Management*, vol. 12, no. 2, pp. 1–13, 2019.

[12] W. T. Dibaba, T. A. Demissie, and K. Miegel, "Prioritization of sub-watersheds to sediment yield and evaluation of best management practices in highland Ethiopia finchaa catchment," *Land*, vol. 106 pages, 2021.

[13] M. L. Berihun, A. Tsunekawa, N. Haregeweyn et al., "Reduced runoff and sediment loss under alternative land capability-based land use and management options in a sub-humid watershed of Ethiopia," *Journal of Hydrology: Regional Studies*, vol. 40, Article ID 100998, 2022.

[14] K. Chimdessa, S. Quraishi, A. Kebede, and T. Alamirew, "Effect of land use land cover and climate change on river flow and soil loss in Didessa River Basin, South West Blue Nile, Ethiopia," *Hydrology*, vol. 6, no. 1, p. 2, 2018.

[15] N. B. Jilo, B. Gebremariam, A. E. Harka, G. W. Woldemariam, and F. Behulu, "Evaluation of the impacts of climate change on sediment yield from the logiya watershed, lower Awash basin, Ethiopia," *Hydrology*, vol. 6, pp. 81–83, 2019.

[16] A. Negese, "Impacts of land use and land cover change on soil erosion and hydrological responses in Ethiopia," *Applied and Environmental Soil Science*, vol. 2021, Article ID 6669438, 10 pages, 2021.

[17] I. Kakarndee and E. Kositsakulchai, "Comparison between swat and swat + for simulating streamflow in a paddy-field-dominated basin , northeast thailand," *E3S Web of Conferences*, vol. 187, p. 06002, 2020.

[18] M. G. Ali, S. Ali, R. H. Arshad et al., "Estimation of potential soil erosion and sediment yield: a case study of the trans-boundary chenab river catchment," *Water (Switzerland)*, vol. 13, no. 24, p. 23, 2021.

[19] A. B. Mitiku, G. A. Meresa, T. Mulu, and A. T. Woldemichael, "Examining the impacts of climate variabilities and land use change on hydrological responses of Awash River basin, Ethiopia," *HydroResearch*, vol. 6, pp. 16–28, 2023.

[20] B. Chelkeba Tumsa, "Statistical and SWAT model-based performance evaluation of RCMs in modeling streamflow and sediment yield at upper Awash sub-basin, Ethiopia," *Applied and Environmental Soil Science*, vol. 2022, Article ID 9193516, pp. 1–19, 2022.

[21] M. F. Baig, M. R. U. Mustafa, I. Baig, H. B. Takaijudin, and M. T. Zeshan, "Assessment of land use land cover changes and future predictions using ca-ann simulation for selangor malaysia," *Water (Switzerland)*, vol. 143 pages, 2022.

[22] B. C. Tumsa, "Performance assessment of six bias correction methods using observed and RCM data at upper Awash basin, Oromia, Ethiopia," *Journal of Water and Climate Change*, vol. 13, no. 2, pp. 664–683, 2022.

[23] X. Du, G. Goss, and M. Faramarzi, "Impacts of hydrological processes on stream temperature in a cold region watershed based on the SWAT equilibrium temperature model," *Water (Switzerland)*, vol. 12, pp. 1112–1114, 2020.

[24] G. T. Ayele, A. K Tebeje, S. S Demissie, and M. A Belete, "Time series land cover mapping and change detection analysis using geographic information system and remote sensing , northern ethiopia," *Air, Soil and Water Research*, vol. 11, 2018.

[25] J. J. Kashaigili and A. M. Majaliwa, "Integrated assessment of land use and cover changes in the Malagarasi river catchment in Tanzania," *Physics and Chemistry of the Earth, Parts A/B/C*, vol. 35, no. 13–14, pp. 730–741, 2010.

[26] E. Koltsida, N. Mamassis, and A. Kallioras, "Hydrological modeling using the SWAT Model in urban and peri-urban environments: the case of Kifissos experimental sub-basin (Athens, Greece)," *Hydrology and Earth System Sciences Discussions*, vol. 2021, pp. 1–24, 2021.

[27] T. Kefay, T. Abdisa, and B. Chelkeba Tumsa, "Prioritization of susceptible watershed to sediment yield and evaluation of best management practice: a case study of awata river, southern Ethiopia," *Applied and Environmental Soil Science*, vol. 2022, Article ID 1460945, 16 pages, 2022.

[28] P. Taylor, P. Chandra, P. L. Patel, P. D. Porey, and I. D. Gupta, "Estimation of sediment yield using swat model for upper tapi basin," *ISH Journal of Hydraulic Engineering*, vol. 20, pp. 37–41, 2015.

[29] T. Zhang, Y. Wang, B. Wang, and P. Feng, "Understanding the main causes of runoffchange by hydrological modeling: a case study in luanhe river basin, north china," *Water*, vol. 108 pages, 2018.

[30] U. A. Sab-basin and M. H. Daba, "Sensitivity of SWAT simulated runoff to temperature and rainfall in the," vol. 9, no. 1, pp. 1–7, 2018.

[31] J. Wu, H. Yen, J. G. Arnold et al., "Development of reservoir operation functions in SWAT+ for national environmental assessments," *Journal of Hydrology*, vol. 583, Article ID 124556, 2020.

[32] K. Bieger, J. G. Arnold, H. Rathjens, M. J. White, D. D. Bosch, and P. M. Allen, "Representing the connectivity of upland areas to floodplains and streams in SWAT+," *Journal of the American Water Resources Association*, vol. 55, no. 3, pp. 578–590, 2019.

[33] J. G. Arnold, D. N. Moriasi, P. W. Gassman et al., "SWAT: model use, calibration, and validation," *Transactions of the ASABE*, vol. 55, no. 4, pp. 1491–1508, 2012.

[34] K. Khanchoul and M. B Jansson, "Sediment rating curves developed on stage and seasonal means in discharge classes for the mellah wadi, Algeria," *Geografiska Annaler - Series A: Physical Geography*, vol. 90, no. 3, pp. 227–236, 2008.

[35] H. Yen, S. Park, J. G. Arnold et al., "IPEAT+: a built-in optimization and automatic calibration tool of SWAT+," *Water (Switzerland)*, vol. 11, no. 8, p. 17, 2019.

[36] N. Resources, H. R. Reduction, and C. Change, *Natural Resources and Environmental Management and Climate Change*, pp. 323–329, Springer, Berlin, Germany, 2009.